Research Article

Atul Raj, Joy Prakash Misra*, Ravinder Pal Singh, Gurminder Singh, Shubham Sharma, and Sayed M. Eldin*

Performance analysis of WEDM during the machining of Inconel 690 miniature gear using RSM and ANN modeling approaches

https://doi.org/10.1515/rams-2022-0288
received October 04, 2022; accepted November 28, 2022

Abstract: The present work aims to carry out a feasible study of wire electro-discharge machining (WEDM) during the machining of Inconel 690 superalloy gears. Processing conditions of power-on time, power-off time, current, and spark-gap voltage are varied to evaluate the process performance in terms of material removal rate (MRR), surface roughness (SR), and wire consumption. Parametric optimization has been carried out using combined approach of response surface methodology (RSM) and artificial neural network (ANN). Results revealed that ANN predicted values are 99% in agreement with the experimental results which validates its effectiveness as compared to RSM predicted values. A viability study of noise characteristics of the processed gear is also done using a noise testing setup. Additionally, FE-SEM has been used to analyze the machined surface's topography. Greater discharge energy brought by a longer pulse length raises the values of MRR, SR, and recast layer thickness (RLT). This study explores the capability of WEDM to produce a more precise and smooth gear profile as compared to other conventional machining methods. Additionally, RLT and microhardness of the machined surface have been critically studied to comprehend the better understanding of the process mechanism.

Keywords: Inconel 690, surface roughness, optimization, gear noise characteristics, response surface methodology, artificial neural network, FE-SEM

*** Corresponding author: Joy Prakash Misra,** Department of Mechanical Engineering, Indian Institute of Technology (BHU), Varanasi, India, e-mail: Jpmisra.mec@iitbhu.ac.in
*** Corresponding author: Sayed M. Eldin,** Faculty of Engineering, Center for Research, Future University in Egypt, New Cairo, 11835, Egypt, e-mail: elsayed.tageldin@fue.edu.eg
Atul Raj: Department of Mechanical Engineering, GD Goenka University, Gurugram, Haryana, India, e-mail: atulraj833@gmail.com
Ravinder Pal Singh: Department of Mechanical Engineering, MMEC, Maharishi Markandeshwar Deemed to be University, Mullana, India, e-mail: ravinderpalsingh89@gmail.com
Gurminder Singh: Department of Mechanical Engineering, Indian Institute of Technology Bombay, Mumbai, India, e-mail: gurmindersingh2012@gmail.com
Shubham Sharma: Mechanical Engineering Department, University Center for Research and Development, Chandigarh University, Mohali, Punjab, 140413, India; School of Mechanical and Automotive Engineering, Qingdao University of Technology, 266520, Qingdao, China, e-mail: shubhamsharmacsirclri@gmail.com, shubham543sharma@gmail.com

1 Introduction

With the advance in micro-electromechanical systems and micro systems, the need for micro-components and micro-devices also increases. For the transmission of motion and power in these micro-systems, there is a need of miniature gears. Miniature gears used in micro-systems have a vast area of application which include miniature motors and pumps, actuators, miniature gearbox, robots, timing mechanism, scientific instruments, aerospace industry, military applications, medical equipment, electronic devices and instruments, etc. [1,2]. Depending on the design and the required quality level, a variety of manufacturing procedures are utilized for the machining of small gears. When machining gears, some of the traditional procedures utilized are hobbing, stamping, extrusion, forging, powder metallurgy, etc. However, in the case of these standard procedures, a secondary finishing operation is necessary to achieve the requisite surface quality of the micro gear, which is a significant disadvantage for them [3]. Electro-spark erosion-based non-conventional machining techniques are now available to help manufacturers produce high-quality small gears with improved surface quality and dimensional precision.

When it comes to machining electrically conductive materials, regardless of their toughness and hardness,

wire electro-discharge machining (WEDM) has become a unique form of electro-spark erosion. It creates surfaces with little grit and has the potential to cut any intricate shape or geometry with great precision. Literature can enlighten readers about important traits, influencing variables, process capacity, etc. [4–7]. The WEDM's material removal method is depicted in Figure 1. For the production of miniature parts for the aerospace sector, dentistry and medical equipment, gear pumps, and motors, among other things, WEDM is frequently utilized. Every machining process has a number of elements that influence how successfully it accomplishes one or more objectives. To improve the process performance, a variety of optimization approaches for single-objective, multi-objective, or both forms of process characteristic optimizations are available.

In the past, Hori and Murtaza used micro- WEDM for the processing of micro spur gear. It was concluded that the micro spur gear has a uniform profile and there was no undercutting error at root area of the gear profile [8]. Benavides *et al.* used micro-WEDM for the machining of 304 SS. Results show that machined surface has micro-level surface finish with good profile characteristics. The thickness of recast layer formed during the machining was also less [9]. Uhlmann *et al.* [10] concluded that micro-WEDM is highly capable of manufacturing miniaturized components with high surface finish and low profile error. Ali *et al.* [11] discussed the comparative study of conventional and WEDM for the fabrication of meso spur gear of copper. It is concluded that gears formed by WEDM process have an average surface roughness (SR) of 1 µm along with the dimensional variation of less than 2%. Talon *et al.* [12] used EDM to manufacture the Ti-6AL-4V spur gear. It was concluded that use of process parameters in a controlled way gives highly precise results. To forecast the value of CS during the WEDM of SiCp/6061 Al metal matrix composite, Shandilya *et al.* employed a combined method of response surface methodology (RSM) and artificial neural network (ANN) [13]. During the WEDM, the wire tool breaking process was investigated by Liao *et al.* During the processing, a computer-aided pulse-discrimination system was cast-off to acquire a large amount of sparking frequency data. The main causes of wire tool breakage were determined to be an excessive spark arc and a sudden increase in the sparking frequency [14]. Paul *et al.* [15] conducted an experimental study on manufacturing of miniature gear of Inconel 718 using WEDM process. Results show that at high discharge energy levels there is a high presence of coral reef on the machined surface, while in case of low discharge energy levels there are random micro-cracks present on the machined surface. Chaubey and Jain [16] studied the microstructure of meso gears machined by WEDM process on a rectangular plate of stainless steel. It was concluded that the gears have uniform tooth profile and are free from the presence of sharp edges at both the end faces. Chaudhary *et al.* [17] conducted a multi-response optimization for miniature gear of Nimonic alloy fabricated by WEDM process using different dielectric fluids. Results reveals that ethylene glycol mixed de-mineralized water used as a dielectric fluid is the most significant parameter among all the input process parameters. Singh and Misra [18] used a combined RSM and ANN technique to examine the surface finish of WEDM-machined combustor material. The predicted and experimental values were found to be in good agreement, proving the validity of the experimental study. Abhilash and Chakradhar have employed the Naive Bayes classifier technique to analyze and categorize the wire rupture during Superalloy 718 machining utilizing WEDM. Short-

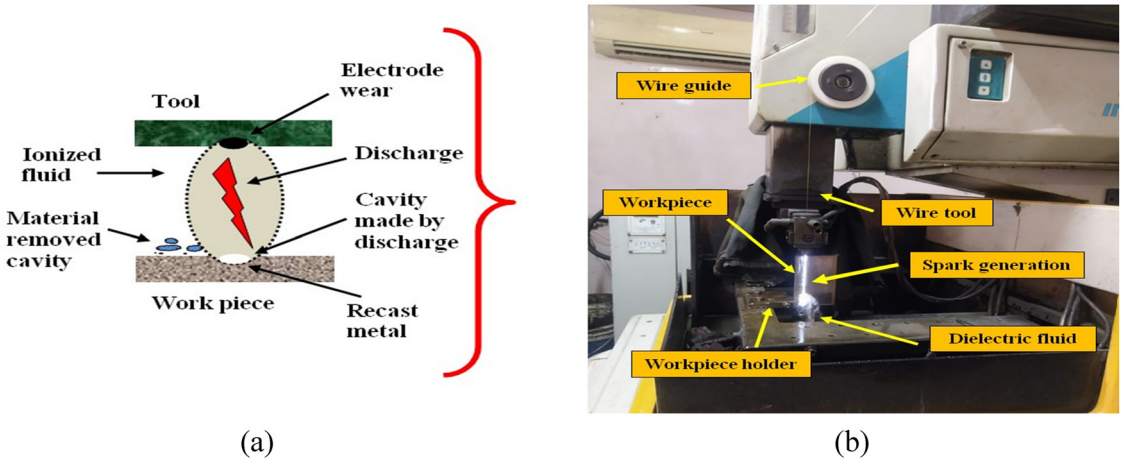

Figure 1: Process mechanism for removing material: (a) schematic and (b) pictorial view.

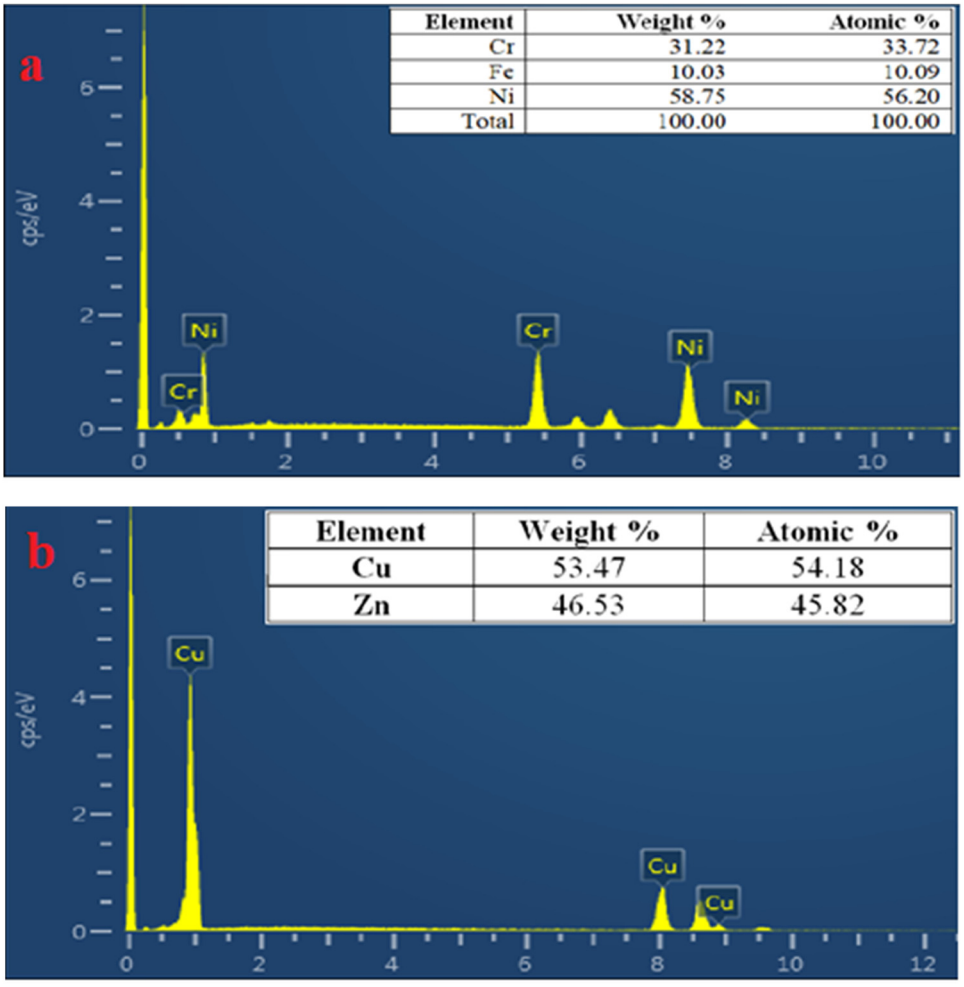

Figure 2: EDS analysis of (a) Inconel 690 and (b) fresh wire.

circuit sparks were found to be the most important factor in wire tool failure [19]. Depending upon the characteristics and its application, various materials like tool-steel, carbon-steel, copper and its alloys, aluminum and its alloys, titanium and its alloys, nickel and its alloys, plastics, nylon, Teflon etc., are used for the manufacturing of miniature gears. Miniature gear made of superalloys has been widely used in aerospace industry, medical implants, electronic industry, gas turbine industry, automobile sector, etc. [20].

Published articles lack any work on formation of miniature gears from nickel-based superalloys and studying the effects of operating conditions on noise characteristics of the gears. Very few authors discuss about the effects of process variables on the tribological behavior of the processed component. So, the present investigation aimed at:

1) Formation of miniature gears from nickel-based superalloy Inconel 690 using WEDM and studying the surface integrity of the tooth profile.
2) Studying the postprocess changes in the surface topography of the processed component by employing scanning electron microscopy (SEM).
3) Analysis of recast layer formation on the gear tooth surface and variation in recast layer thickness (RLT) along the machined surface using FE-SEM.
4) RSM and ANN-based multi-objective process variable optimization
5) Studying the effects of operating conditions on the gear noise characteristics.

2 Materials and methodology

2.1 Materials

In the present study a nickel-based superalloy Inconel 690 is used as the workpiece material. Inconel 690 has

high chromium content in it which offers high strength and high corrosion resistance property in aqueous medium and high temperature. It has immense demand in industrial area and is very much needed in aerospace and gas turbine industry. A rectangular plate with dimensions 150 mm × 150 mm × 15 mm is used for the manufacturing of miniature gears. Miniature spur gears with outer diameter of 10 mm are cut from the rectangular plate. EDS analysis of the workpiece material and wire tool is demonstrated in Figure 2, respectively.

2.2 Methodology

In the present study, WEDM machine (Model: Sprint cut-ELECTRONICA) is used for the cutting of miniature gears from the workpiece surface. Superalloy 690 is a very hard material to cut because of its high strength and hardness. A pictorial view of the process followed during the present study is shown in Figure 3. Initially, grinding and buffing of workpiece plate is done to remove the layer of impurities present on its surface in order to avoid the wire breakage and proper spark generation during WEDM. In the present analysis, power-on time (T_{on}), power-off time (T_{off}), peak current (I_p), and spark gap voltage (S_v) are used as input process variables. Process performance is evaluated in respect of material removal rate (MRR), SR, and wire consumption (WC). Ranges and level of input process variables are tabulated in Table 1.

In the next step, an experimental plan is set for accomplishment of the experiments using WEDM with the help of Box–Behnken design (BBD) of RSM [21–24]. Although the central composite design (CCD) has been chosen in various past research [25–29], BBD was chosen over CCD as it provides lesser number of experiments for

Figure 3: Pictorial view of process flow chart: (a) WEDM machine setup, (b) processing of superalloy 690 by WEDM, (c and d) miniature spur gears and their cavity in the plate after WEDM, (e) SR measurement, and (f) microhardness analysis.

Table 1: Ranges and levels of input variables

Variables	Input process parameters					
	Source	Range	Unit	Level		
				1	2	3
Power-on time (T_{on})	A	105–131	µs	105	118	131
Power-off time (T_{off})	B	30–60	µs	30	45	60
Peak current (I_p)	C	40–220	A	40	130	220
Spark gap voltage (S_v)	D	20–80	V	20	50	80

same number of parameters. As per Box behnken design, a total of 29 runs are done with 5 replications of center shown in Table 2. The manufacturing of miniature gears from the super alloy 690 square plate using WEDM is shown in Figure 3(c). Following WEDM processing, the SR of the miniature gears is measured using a Telesurf surfcom (Make: Accretech) roughness tester. The treated surface's roughness is measured according to ISO 1997 standards. The calculations used a cut-off value of 2.5 m and a sampling length of 4 mm. Five tests were run on each machined surface, and the average result was used to determine the roughness value. FE-SEM (Make: Joel, JSM-6390LV, 20.0 keV) was used for microstructural investigation, and Vickers' hardness tester was used for microhardness measurement [30–32].

3 Results and discussion

T_{on}, T_{off}, I_p, and S_v are selected as input factors for the current study, while MRR, SR, and WC are regarded as response variables. The effects of various input factors on process performance are depicted in Figure 4. Among all the input factors, T_{on} is discovered to have the greatest influencing power. The output data demonstrate that as T_{on} increases, MRR and SR also rise and *vice versa*. The number of electrons striking the work surface in a single

Table 2: Experimental runs

No. of runs	Input process variables				Experimental results			RSM predicted			ANN predicted		
	T_{on}	T_{off}	I_p	S_v	MRR	SR	WC	MRR	SR	WC	MRR	SR	WC
1	A1	B1	C2	D2	3.83	1.64	42.98	9.17	1.67	51.46	3.83	1.67	42.97
2	A3	B1	C2	D2	6.67	3.82	19.56	14.6	3.69	30.00	9.03	3.55	17.90
3	A1	B3	C2	D2	1.27	0.73	144.92	4.85	0.81	137.26	1.28	0.81	144.66
4	A3	B3	C2	D2	5.55	3.18	31	11.7	3.10	25.30	5.54	3.12	31.08
5	A2	B2	C1	D1	4.2	2.46	40.09	6.34	2.25	47.91	9.09	1.48	18.50
6	A2	B2	C3	D1	6.11	3.11	27.17	15.7	3.06	25.91	6.10	3.06	27.32
7	A2	B2	C1	D3	2.34	1.54	71.75	4.23	1.54	75.79	2.31	1.59	71.47
8	A2	B2	C3	D3	6.42	2.85	25.79	15.8	3.01	20.75	9.04	2.84	18.06
9	A1	B2	C2	D1	2.23	1.63	78.11	8.30	1.43	77.47	3.34	0.94	73.32
10	A3	B2	C2	D1	6.67	3.02	28.22	13.8	3.09	22.13	6.71	3.25	28.22
11	A1	B2	C2	D3	1.68	0.72	94.8	6.60	0.55	100.2	1.49	0.86	94.56
12	A3	B2	C2	D3	7.47	3.11	22.15	13.4	3.21	22.11	7.47	3.18	22.02
13	A2	B1	C1	D2	4.64	2.39	36.42	6.65	2.36	33.31	7.96	2.39	20.64
14	A2	B3	C1	D2	1.6	1.82	105.14	3.04	1.92	101.44	1.76	1.69	104.01
15	A2	B1	C3	D2	4.84	3.98	19.34	17.1	3.79	22.37	4.82	3.84	19.39
16	A2	B3	C3	D2	5.18	2.83	32.91	13.55	2.77	35.34	5.18	2.78	32.93
17	A1	B2	C2	D2	1.36	0.47	130.65	2.49	0.58	126.39	1.33	0.81	116.33
18	A3	B2	C1	D2	3.98	2.51	43.1	6.30	2.51	42.33	4.07	2.44	42.63
19	A1	B2	C3	D2	2.41	1.39	71.85	10.62	1.50	70.53	2.44	1.38	71.87
20	A3	B2	C3	D2	6.86	3.88	18.98	19.19	3.88	21.15	6.83	3.81	18.97
21	A2	B1	C2	D1	5.14	2.81	32.5	12.09	3.07	24.22	5.16	2.74	32.65
22	A2	B3	C2	D1	7.28	2.54	32.95	10.92	2.63	41.40	7.27	2.55	33.13
23	A2	B1	C2	D3	5.14	2.96	22.75	13.50	2.98	12.21	5.15	2.84	22.76
24	A2	B3	C2	D3	2.42	2.11	69.94	7.47	1.96	76.13	2.42	2.15	70.11
25	A2	B2	C2	D2	9.38	2.83	17.96	14.48	2.31	18.13	8.65	2.39	18.22
26	A2	B2	C2	D2	8.34	2.08	18.46	14.48	2.31	18.13	8.65	2.39	18.22
27	A2	B2	C2	D2	8.26	2.17	17.63	14.48	2.31	18.13	8.65	2.39	18.22
28	A2	B2	C2	D2	8.37	2.29	18.35	14.48	2.31	18.13	8.65	2.39	18.22
29	A2	B2	C2	D2	8.38	2.22	18.22	14.48	2.31	18.13	8.65	2.39	18.22

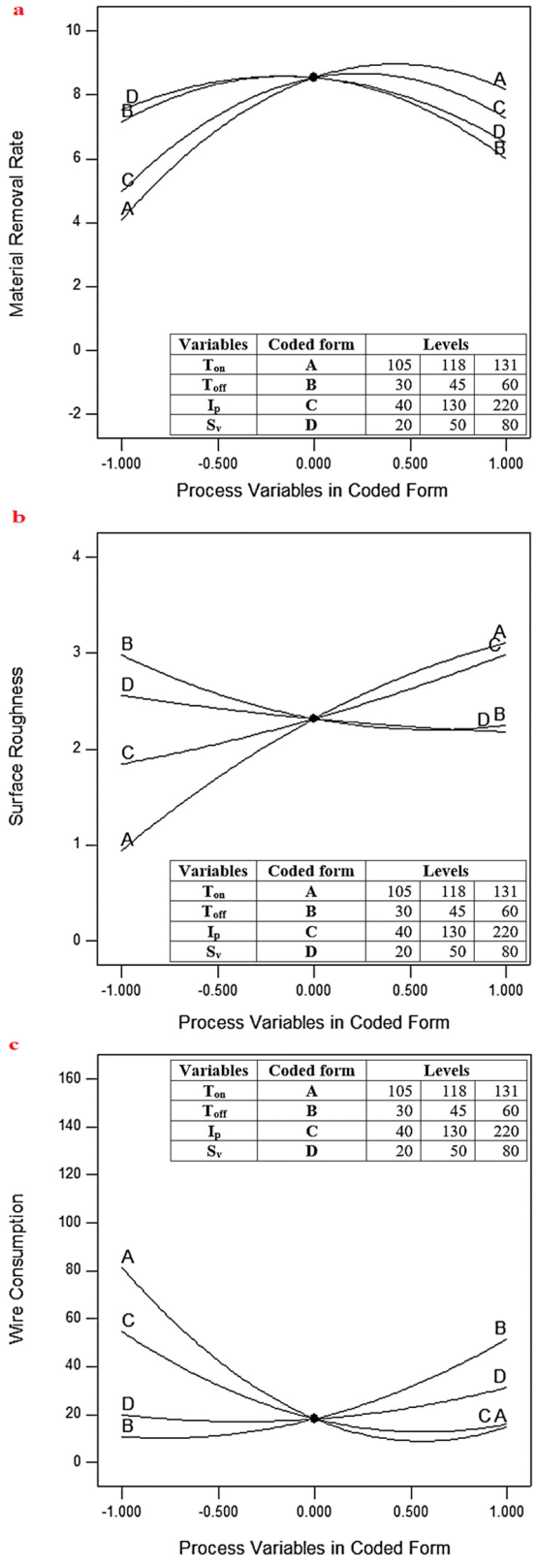

Figure 4: Various input factors' effect on: (a) MRR, (b) SR, and (c) WC.

discharge increases as T_{on} and I_p grow. More materials are removed from the work surface for each discharge. As a result, MRR rises as T_{on} and I_p rises. The metal is removed from the work surface in the form of craters, which is a well-known phenomenon of WEDM. Increased material removal results in a poor surface finish and a higher SR value. On the other hand, WC has a different response as compared to MRR and SR for T_{on} [33–35]. High discharge energy is associated with higher T_{on} and I_p values. As a result, the wire tool length required to eradicate the material from the work piece is reduced. As the wire feed remains constant throughout the process, T_{off} increases the pulse duration, requiring more wire tool length to eradicate the material from the work piece. A larger S_v widens the space between the work piece and the wire tool, resulting in reduced spark concentration. As a result, the amount of wire used increases. It is obvious from the results that I_p also has similar possessions like T_{on} on MRR, SR, and WC. T_{off} and S_v also have some severe effects on MRR, SR, and WC [36–38]. As the T_{off} and S_v value drops, some rise in the value of MRR and SR is noticed.

The time period of sparks creation in the WEDM process increases with the increase in T_{on} value, which inexorably influences the MRR. The spark gap narrows as the S_v decreases, increasing the number of sparks produced per unit of time. The machining rate is indirectly accelerated, increasing the MRR [39–41]. The findings show that higher T_{on} and I_p values result in increased MRR and SR. According to interaction plots, the increase in T_{on} and I_p values is predominantly associated with an increase in MRR; however, after reaching a certain point, MRR begins to decline. Though, as seen in Figure 4a, MRR for T_{off} and S_v declines as their values increase. According to the findings for SR, which are depicted in Figure 4b, SR rises as T_{on} and I_p values increase.

3.1 Multi-objective optimization

ANN is a MATLAB toolkit. Backpropagation neural network (BPNN) models are commonly created with it. WEDM has a large sum of input process factors which have a

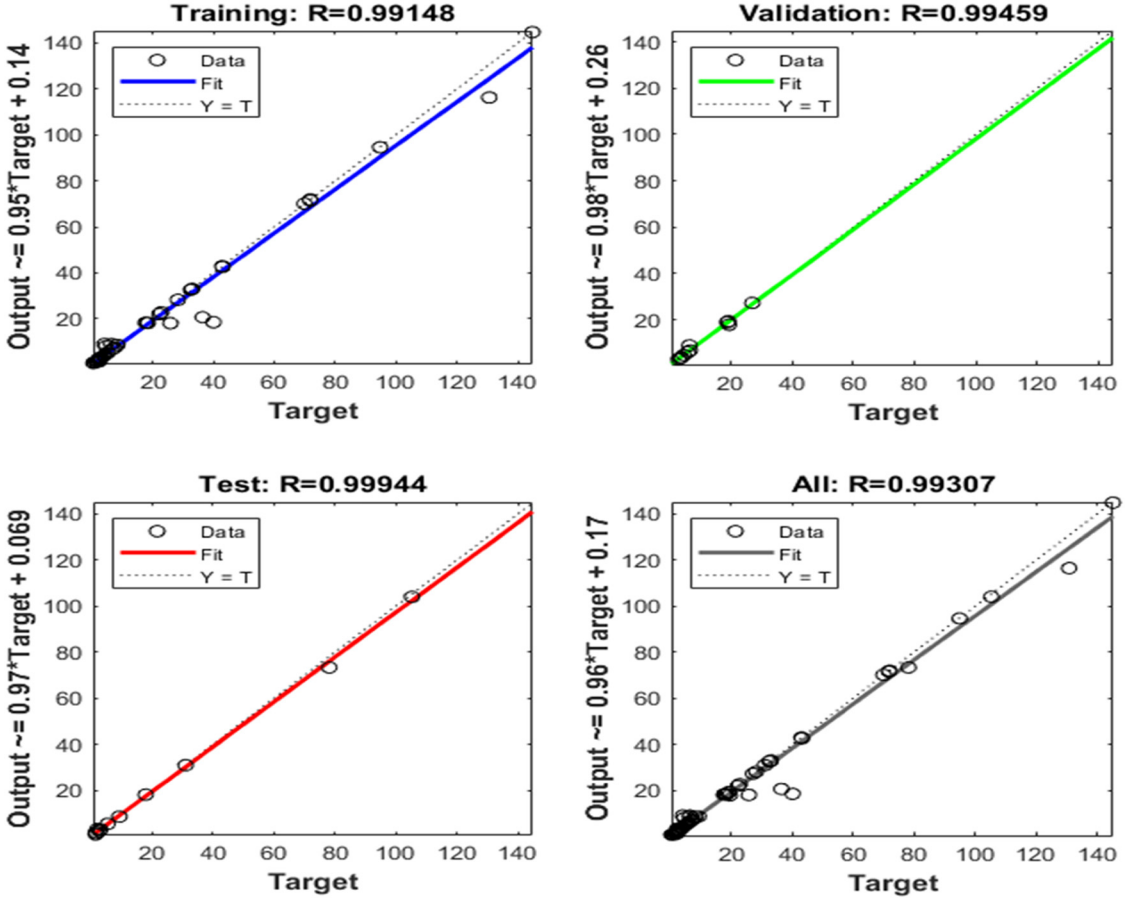

Figure 5: Comparative graph of actual and ANN projected values, using linear regression analysis.

substantial impact on the process output. Because of the intricacy and stochastic nature of the data, statistical analysis is possible, but precise guess of values using a scientific equation is not valid. As a training vector, four input process variables are included in the current study.

Various limitations, such as the number of iterations, hidden layer nodes, network type, and so on, affect the performance of a BPNN model. As a result, during BPNN training, selecting the most optimal values for input process variables is crucial [30].

The ideal configuration of the ANN model is determined for current study by altering the sum of neurons in the hidden layer. For the current ANN model, the dataset is split into three parts: 60% for training, 20% for validation, and 20% for testing. The current model is an FF-BPNN with a Levenberg–Marquardt training procedure. In the existing model, 1 buried layer contains 20 neurons. The linear regression graphs of actual vs predicted values for ANN are shown in Figure 5. The *R*-values achieved for the training and validation datasets in this model are 0.99148 and 0.99459, respectively, which are extremely near to 1. The current model's results reveal that actual and anticipated values are in good agreement. In addition, Figure 6 shows a comparison graph between the actual values and the expected outcomes. In comparison to the quadratic RSM model, the constructed ANN model provides more exact and generalized predicted values, as seen in the comparison graph.

4 Surface topography and noise characteristics analysis

4.1 Surface integrity

Investigation of profile characteristics on the WEDM small gear profile reveals the existence of micro-cracks and bowl-shaped cavities called craters on the gear tooth surface, as well as some spherical droplets [42–44]. Some molten metal and re-solidified material can also be seen on the gear tooth surface in the form of a lump of debris. Figure 7 shows a burr-free uniform tooth profile of WEDMed gears machined under various operating circumstances, as

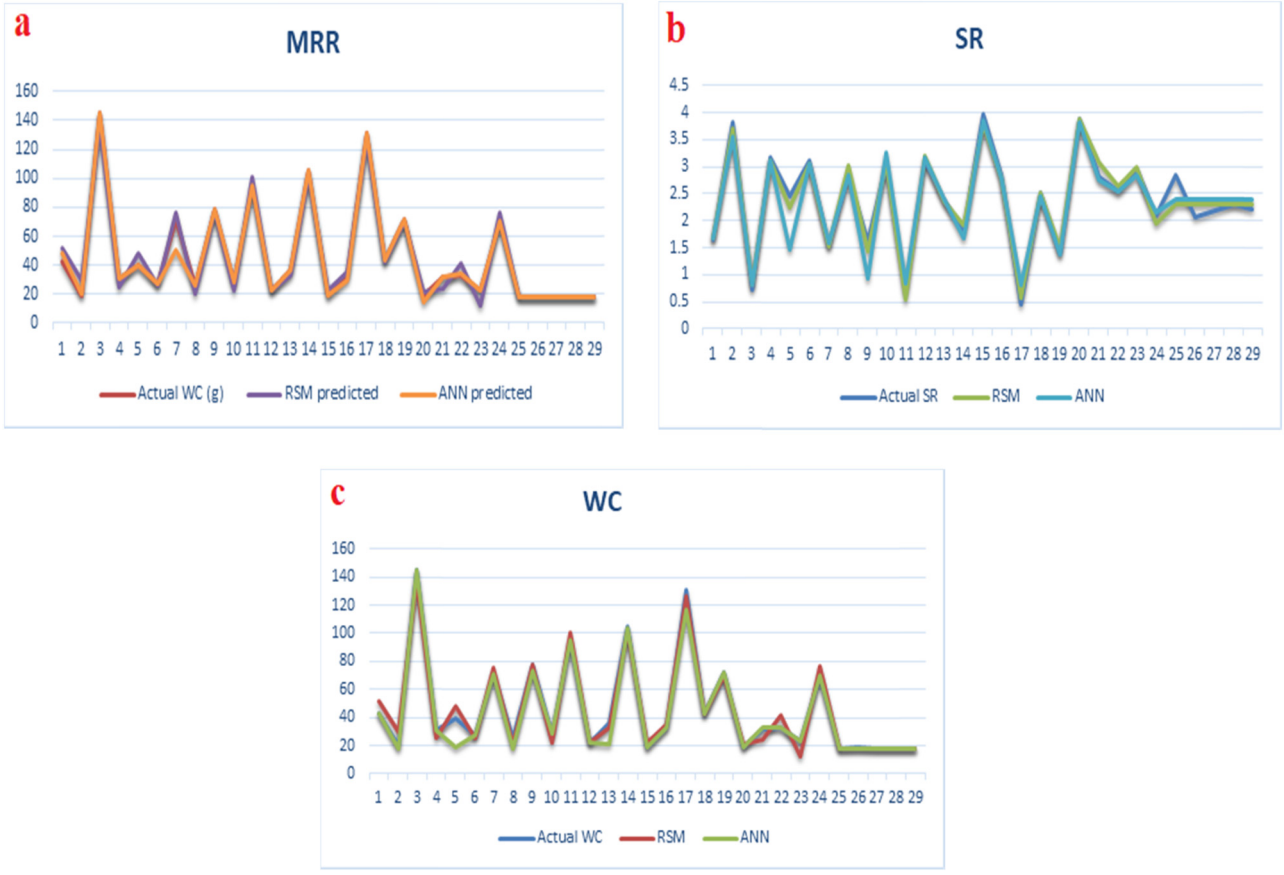

Figure 6: Relative graph of actual vs predicted values for (a) MRR, (b) SR, and (c) WC.

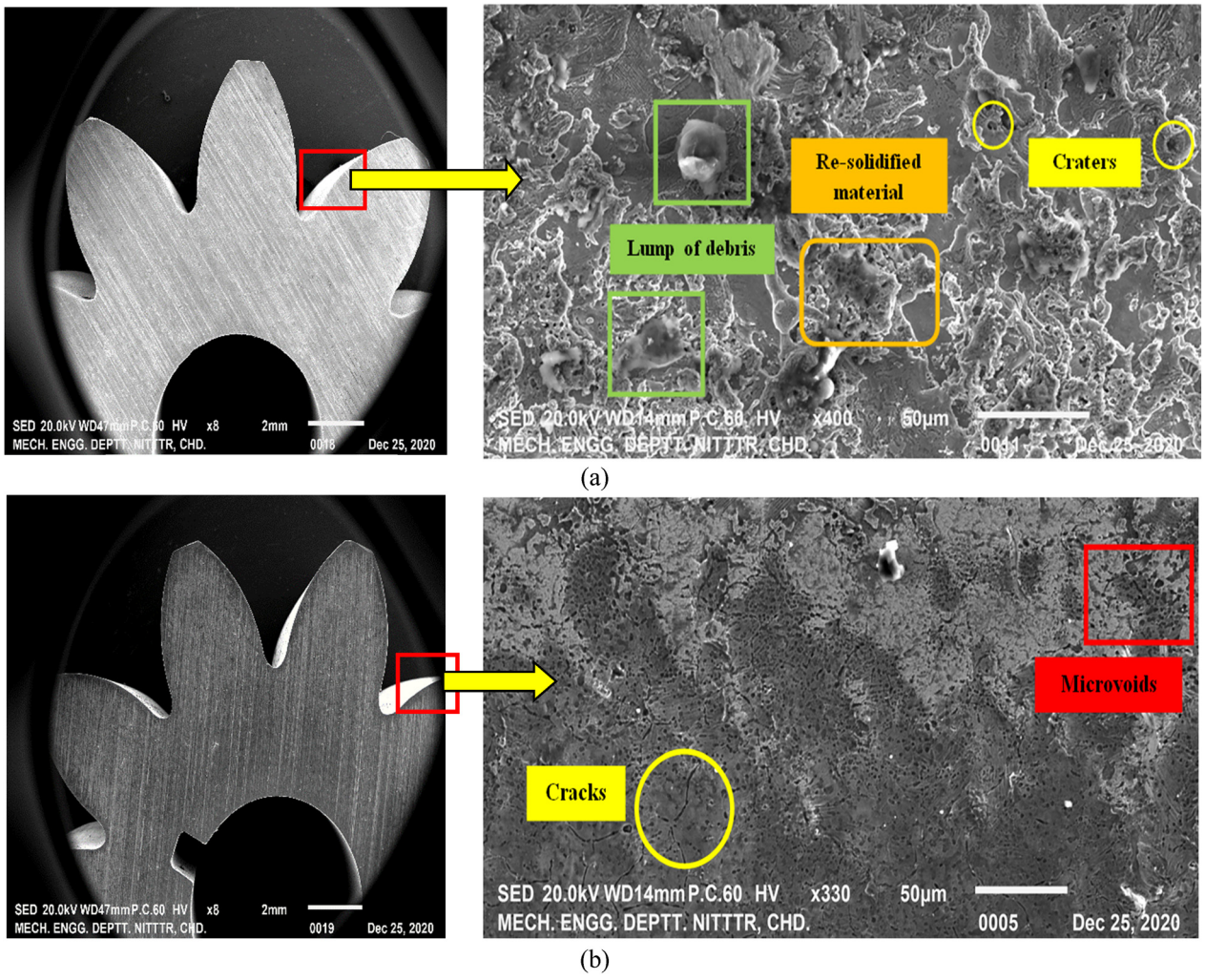

Figure 7: SEM micrographs of gear profile and gear tooth surface machined at (a) T_{on}, 118; T_{off}, 30; I_p, 220; S_v, 50 and (b) T_{on}, 105; T_{off}, 45; I_p, 130; S_v, 50.

well as their microstructures. Small craters, spherical modules with a lump of debris, and re-solidified material are portrayed on the surface of the machined work piece, according to Figure 7a and b.

4.2 Microhardness analysis

The hardness of the work piece is affected by the formation of recast layers on its top surface. Testing for microhardness is an easy technique to confirm this. In this work, a microhardness testing machine is used to examine the variation in the microhardness values of the core material and the machined region [45,46]. The variance in microhardness along the subsurface of the recast layer is seen in Figure 8. In comparison to the core materials, microhardness rises close to the subsurface of the recast layer, as depicted in the graphs. The formation of recast layers on the face of the processed work surface enhances the hardness of the work piece. Because the recast layer is formed exclusively on the machined area of the work piece, the hardness of the core material is not affected. A total of six indentations have been made on each work surface, starting from one end to the other end, as shown in Figure 8. From the results, it can be seen that the value of hardness decreases as the testing point moves from machine area to the core area of the processed work piece.

4.3 Noise characteristics

These types of problems significantly reduce the gear's service life. The setup used for noise measurement, as

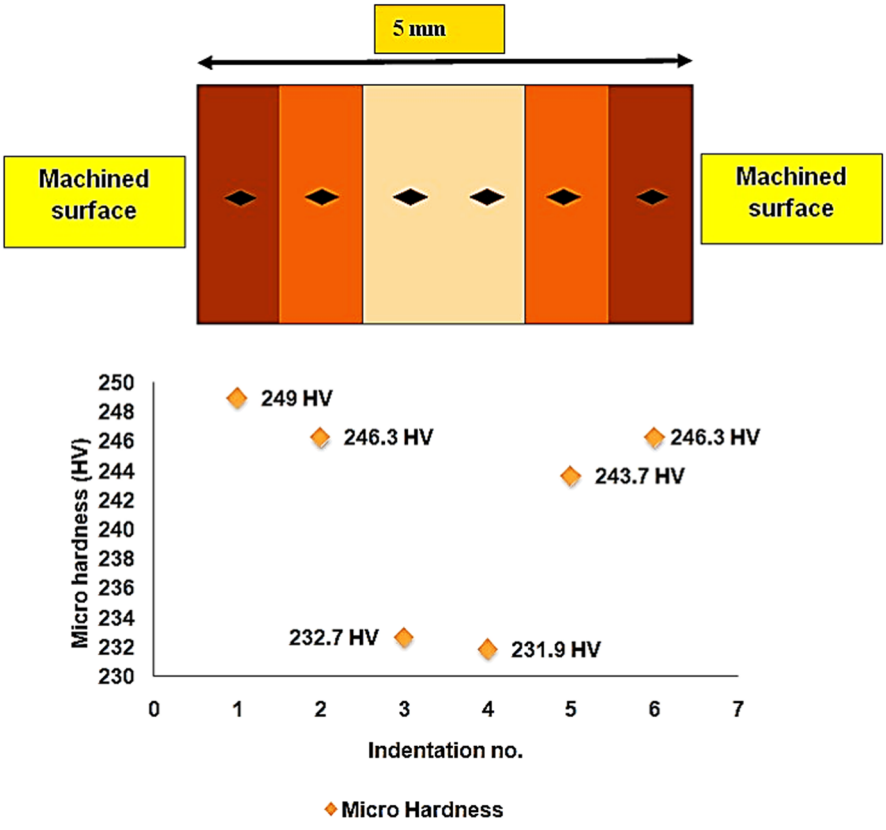

Figure 8: Microhardness analysis.

shown in Figure 9, comprises of a pair of spur gear in which one is the master gear and the other one is the testing gear. The noise generated during the meshing of the gears was measured at different time intervals. A DC motor, which is used to supply power, is connected to the master gear. Master gear can rotate from 1,500 to 2,800

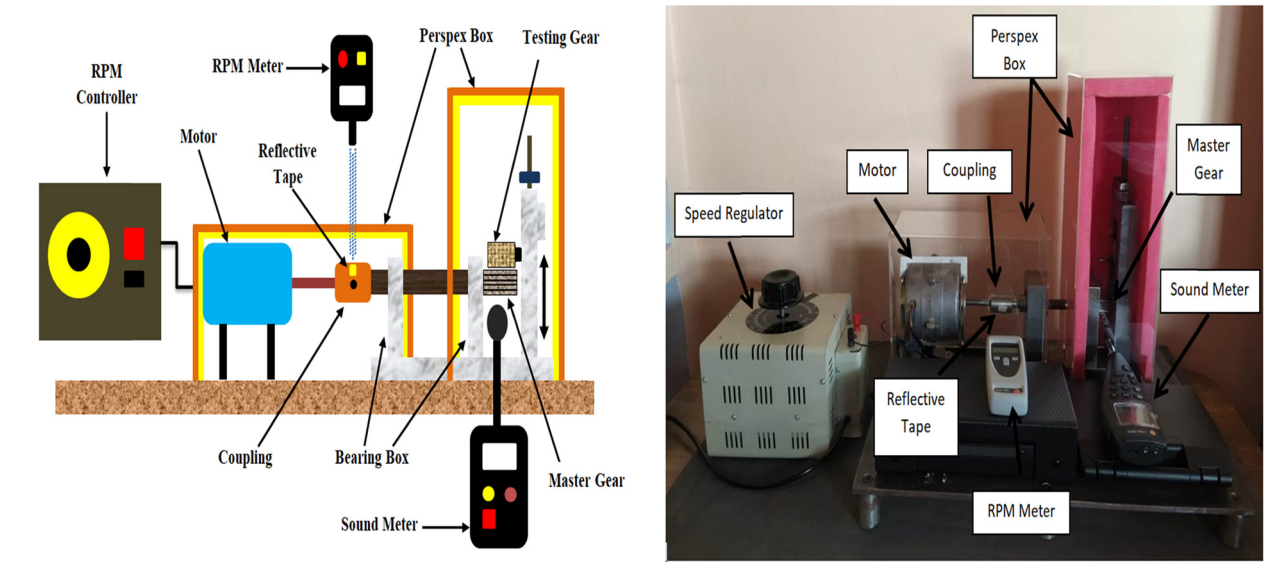

Figure 9: Noise testing setup: (a) schematic view and (b) photographic view.

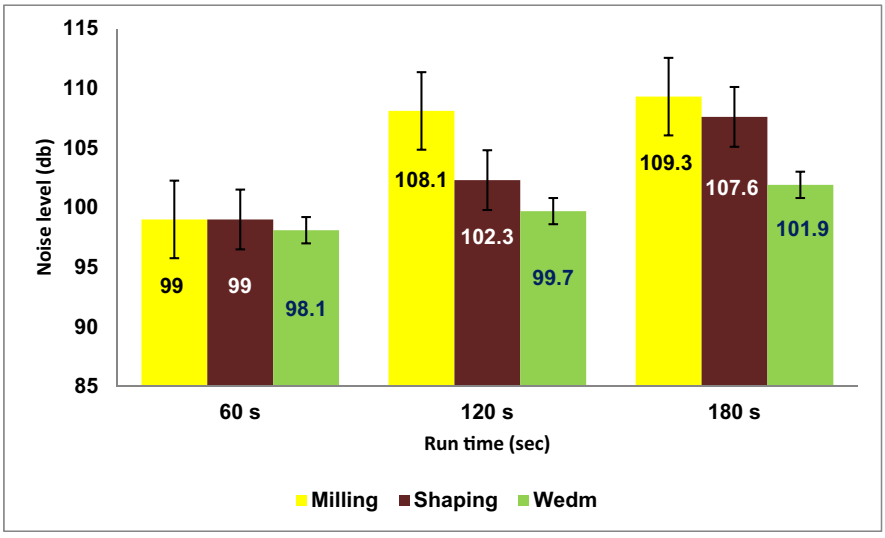

Figure 10: Comparative graph of noise level for milling, shaping, and WEDM processed gears.

RPM. The speed of the master gear can be varied with the help of the RPM controller. Two Perspex boxes are used, one is to cover the power supply chamber, i.e., motor and the other one for the gear meshing chamber to avoid the sound of the surroundings.

A non-contact RPM meter, i.e., testo-465 with a measuring range of +1 to +99,999 RPM and accuracy of ±0.02% of the measured value is used for monitoring the speed of rotation. For noise measurement, a sound level meter, i.e., testo 816-1 with a measuring range of 30–130 dB is used. A comparative study between gears manufactured by two different conventional processes, i.e., milling and shaping is done to analyze the effects of machining process on the noise characteristics of the gear. Both the gears are meshed with the master gear individually for different run time, and during the meshing period, their noise levels are recorded using sound level meter [47,48]. Noise level of gear manufactured through milling process is higher as compared to that of gear manufactured through shaping process. Initially, the sound level for both the processes was approximately 99 dB for a run time of 60 s. As the run time increases, the difference between the noise levels of both the processes also increases. In case of WEDM machined gears, noise was measured at three different levels of time, i.e., 60, 120 and 180 s respectively. In case of 60 s, maximum level of noise generated by the meshing gears is 98 dB, while in case of 120 s meshing time, the maximum noise level is 99.7 dB. For 180 s meshing time, the noise level reaches up to 102 dB.

From the experimental results, it was concluded that with the increase in the meshing time, the noise and vibration also increases, but when compared to the conventional machining processes, the gear manufactured by WEDM process generates less noise [49,50]. A comparative graph of both the conventional methods with WEDM process is shown in Figure 10. Average noise levels for milling, shaping, and WEDM processed gears at different run time are shown in Table 3.

Table 3: Noise level results at different intervals of time

S. No	Gears	Average noise levels		
		60 s	120 s	180 s
1	Milling gear	99.40 dB	108.12 dB	109.38 dB
2	Shaper gear	99.42 dB	102.37 dB	107.60 dB
3	WEDM gear	98.13 dB	99.75 dB	101.91 dB

5 Conclusion

The present study accomplishes that the gear tooth profile, which was machined at different parametrical settings (maximum MRR and SR conditions), has small craters and spherical modules with a lump of debris and re-solidified materials on its surface, according to surface integrity analysis. As there are fewer craters and less amount of debris on the surface of the machined surface under minimum MRR and SR parametrical settings, this surface is found to be smoother. From experimental runs, it was concluded that, among all the input process variables, pulse-on time (T_{on}) is the most significant variable

which affects the process performance mostly. When BPNN models are compared to quadratic RSM models, it is found that the generated BPNN models have more precision and accuracy. Noise characteristic analysis shows that with the increase in the meshing time, the gear noise level also increases. From the comparative analysis, it is clear that the gears machined by WEDM process have good micro-geometry and high surface quality as compared to that manufactured by conventional gear manufacturing processes.

Acknowledgments: The researchers would like to thank Research Facility Cell, National Institute of Technology Kurukshetra for their support and guidance.

Funding information: The authors state no funding involved.

Author contributions: Conceptualization: Atul Raj, Joy Prakash Misra, Ravinder Pal Singh, Gurminder Singh, and Shubham Sharma; formal analysis: Atul Raj, Joy Prakash Misra, Ravinder Pal Singh, Gurminder Singh, and Shubham Sharma; investigation: Atul Raj, Joy Prakash Misra, Ravinder Pal Singh, Gurminder Singh, and Shubham Sharma; writing – original draft preparation: Atul Raj, Joy Prakash Misra, Ravinder Pal Singh, Gurminder Singh, and Shubham Sharma; writing – review and editing: Shubham Sharma and Sayed M. Eldin; supervision: Shubham Sharma and Sayed M. Eldin; project administration: Shubham Sharma and Sayed M. Eldin; and funding acquisition: Shubham Sharma and Sayed M. Eldin. All authors have accepted responsibility for the entire content of this manuscript and approved its submission.

Conflict of interest: The authors state no conflict of interest.

Data availability statement: The datasets generated during and/or analysed during the current study are available from the corresponding author on reasonable request.

References

[1] Jain, N. K. and S. K. Chaubey. *Review of miniature gear manufacturing*, Comprehensive Materials Finishing. Elsevier Inc., Oxford, UK, Vol. 1–3, 2017. ISBN 9780128032503.

[2] Singh, S., G. Singh, C. Prakash, S. Ramakrishna, L. Lamberti, and C. I. Pruncu. 3D printed biodegradable composites: An insight into mechanical properties of PLA/chitosan scaffold. *Polymer Testing*, Vol. 89, 2020, id. 106722.

[3] Raj, A. and J. P. Misra. Challenges and opportunities in ECH of gears. *Materials Science Forum*, Vol. 969 MSF, 2019, pp. 595–600.

[4] Bobbili, R., V. Madhu, and A. K. Gogia. Effect of wire-EDM machining parameters on surface roughness and material removal rate of high strength armor steel. *Materials and Manufacturing Processes*, Vol. 28, 2013, pp. 364–368.

[5] Mouralova, K., J. Kovar, L. Klakurkova, J. Bednar, L. Benes, and R. Zahradnicek. Analysis of surface morphology and topography of pure aluminium machined using WEDM. *Measurement*, Vol. 114, 2018, pp. 169–176.

[6] Mussada, E. K., C. C. Hua, and A. K. P. Rao. Surface hardenability studies of the die steel machined by WEDM. *Materials and Manufacturing Processes*, Vol. 33, 2018, pp. 1745–1750.

[7] Sharma, N., R. Khanna, and R. Gupta. Multi quality characteristics of WEDM process parameters with RSM. *Procedia Engineering*, Vol. 64, 2013, pp. 710–719.

[8] Hori, K. and Y. Murtaza. Wire electrical discharge machining of micro-involute gears. *Transactions of the Japan Society of mechanical engineers*, Vol. 57, 1977, pp. 364–370.

[9] Benavides, G. L., L. F. Bieg, M. P. Saavedra, and E. A. Bryce. High aspect ratio meso-scale parts enabled by wire micro-EDM. *Microsystem Technologies*, Vol. 8, 2002, pp. 395–401.

[10] Uhlmann, E., S. Piltz, and U. Doll. Machining of micro/miniature dies and moulds by electrical discharge machining - recent development. *Journal of Materials Processing Technology*, Vol. 167, 2005, pp. 488–493.

[11] Ali, M. Y., A. N. Mustafizul Karim, E. Y. T. Adsesta, A. F. Ismail, A. A. Abdullah and M. N. Idris. Comparative study of conventional and micro WEDM based on machining of meso/micro sized spur gear. *International Journal of Precision Engineering and Manufacturing*, Vol. 11, 2010, pp. 779–784.

[12] Huertas Talón, J. L., J. C. Cisneros Ortega, C. López Gómez, E. Ros Sancho, and E. Faci Olmos. Manufacture of a spur tooth gear in Ti-6Al-4V alloy by electrical discharge. *Computer-Aided Design*, Vol. 42, 2010, pp. 221–230.

[13] Shandilya, P., P. K. Jain, and N. K. Jain. RSM and ANN modeling approaches for predicting average cutting speed during WEDM of SiCp/6061 Al MMC. *Procedia Engineering*, Vol. 64, 2013, pp. 767–774.

[14] Liao, Y. S., Y. Y. Chu, and M. T. Yan. Study of wire breaking process and monitoring of WEDM. *International Journal of Machine Tools and Manufacture*, Vol. 37, 1997, pp. 555–567.

[15] Paul, T., S. Chakraborty, N. K. Mandal, and D. Bose. An experimental investigation on development of miniature spur gear by WEDM of inconel 718. *Proceedings of. 6th International & 27th All India Manufacturing Technology, Design and Research Conference* (*AIMTDR-2016*), 2016, pp. 1523–1527.

[16] Chaubey, S. K. and N. K. Jain. Investigations on microgeometry of meso bevel and meso helical gears manufactured by WEDM process. *The International Journal of Advanced Manufacturing Technology*, Vol. 93, 2017, pp. 4217–4231.

[17] Chaudhary, T., A. N. Siddiquee, A. K. Chanda, M. H. Abidi, and A. Al-Ahmari. Multi-response optimization for nimonic alloy miniature gear fabrication using wire electrical discharge machining. *Advances in Mechanical Engineering*, Vol. 12, 2020, pp. 1–13.

[18] Singh, B. and J. P. Misra. Surface finish analysis of wire electric discharge machined specimens by RSM and ANN Modeling. *Measurement*, Vol. 137, 2019, pp. 225–237.
[19] Abhilash, P. M. and D. Chakradhar. Sustainability improvement of WEDM process by analysing and classifying wire rupture using kernel-based naive bayes classifier. *Journal of the Brazilian Society of Mechanical Sciences and Engineering*, Vol. 43, 2021, pp. 1–9.
[20] Singh, B. and J. P. Misra. Process regulations and mechanism of WEDM of combustor material. *SAE International Journal of Aerospace*, Vol. 12, 2019, pp. 77–96.
[21] Myers, R. H. and D. C. Montgomery. Response surface methodology: Process and product optimization using designed experiments. *Journal of Statistical Planning and Inference*, 59, 1997, pp. 185–186.
[22] Batra, N. K., R. P. Singh, and S. Dayal. Experimental investigation and statistical modelling of cutting speed in AL6063-W composite by wire EDM process. *Materials Today: Proceedings*, Vol. 62, 2022, pp. 1408–1412.
[23] Pal Singh, R., N. K. Batra, and S. Dayal. Influence of machining parameters on surface roughness in AL6063-W composite by wire EDM Process: Experimental investigations and process optimization. *Materials Today: Proceedings*, Vol. 63, 2022, pp. 192–196.
[24] Singh, G., S. Singh, J. Singh, and P. M. Pandey. Parameters effect on electrical conductivity of copper fabricated by rapid manufacturing. *Materials and Manufacturing Processes*, 2020, pp. 1–12.
[25] Singh, G. and P. M. Pandey. Rapid manufacturing of copper components using 3D Printing and ultrasonic assisted pressureless sintering: Experimental investigations and process optimization. *Journal of Manufacturing Processes*, Vol. 43, 2019, pp. 253–269.
[26] Singh, S., G. Singh, K. Sandhu, C. Prakash, and R. Singh. Investigating the optimum parametric setting for MRR of expandable polystyrene machined with 3D printed end mill tool. *Materials Today: Proceedings*, Vol. 33, 2020, pp. 1513–1517.
[27] Dikshit, I., G. Bhushan, R. P. Singh, and N. K. Batra. Statistical modeling and optimization of density in a novel carbon/jute fiber reinforced hybrid composite. *Materials Today: Proceedings*, Vol. 63, 2022, pp. 259–263.
[28] Singh, R. P., P. Mohan, and A. Ranjan. An *in-vitro* study of temperature rise during rotary ultrasonic bone drilling of human bone. *Medical Engineering & Physics*, Vol. 79, 2020, pp. 33–43.
[29] Singh, R. P., P. M. Pandey, A. R. Mridha, and T. Joshi. Experimental investigations and statistical modeling of cutting force and torque in rotary ultrasonic bone drilling of human cadaver bone. *Proceedings of the Institution of Mechanical Engineers, Part H: Journal of Engineering in Medicine*, Vol. 234, 2020, pp. 148–162.
[30] Desai, K. M., B. K. Vaidya, R. S. Singhal, and S. S. Bhagwat. Use of an artificial neural network in modeling yeast biomass and yield of β-Glucan. *Process Biochemistry*, Vol. 40, 2005, pp. 1617–1626. doi: 10.1016/j.procbio.2004.06.015.
[31] Sheng, C., G. He, Z. Hu, C. Chou, J. Shi, J. Li, et al. Yarn on yarn abrasion failure mechanism of ultrahigh molecular weight polyethylene fiber. *Journal of Engineered Fibers and Fabrics*, Vol. 16, 2021, id. 1925832385.
[32] Ning, F., G. He, C. Sheng, H. He, J. Wang, R. Zhou, et al. Yarn on yarn abrasion performance of high modulus polyethylene fiber improved by graphene/polyurethane composites coating. *Journal of Engineered Fibers and Fabrics*, 2021, Vol. 16, pp. 1–10.
[33] Lv, B., S. Wang, T. Xu, and F. Guo. Effects of minor Nd and Er additions on the precipitation evolution and dynamic recrystallization behavior of Mg–6.0Zn–0.5Mn alloy. *Journal of Magnesium and Alloys*, Vol. 9, No. 3, 2021, pp. 840–852.
[34] Zhang, B., Z. Wang, H. Yu, and Y. Ning. Microstructural origin and control mechanism of the mixed grain structure in Ni-based superalloys. *Journal of Alloys and Compounds*, Vol. 900, 2022, id. 163515.
[35] Liang, L., M. Xu, Y. Chen, T. Zhang, W. Tong, H. Liu, et al. Effect of welding thermal treatment on the microstructure and mechanical properties of nickel-based superalloy fabricated by selective laser melting. *Materials science & engineering A, Structural Materials: Properties, Microstructure and Processing*, Vol. 819, 2021, id. 141507.
[36] Xie, J., Y. Chen, L. Yin, T. Zhang, S. Wang, and L. Wang. Microstructure and mechanical properties of ultrasonic spot welding TiNi/Ti6Al4V dissimilar materials using pure Al coating. *Journal of Manufacturing Processes*, Vol. 64, 2021, pp. 473–480.
[37] Deng, H., Y. Chen, Y. Jia, Y. Pang, T. Zhang, S. Wang, et al. Microstructure and mechanical properties of dissimilar NiTi/Ti6Al4V joints via back-heating assisted friction stir welding. *Journal of Manufacturing Processes*, Vol. 64, 2021, pp. 379–391.
[38] Yuhua, C., M. Yuqing, L. Weiwei, and H. Peng. Investigation of welding crack in micro laser welded NiTiNb shape memory alloy and Ti6Al4V alloy dissimilar metals joints. *Optics & Laser Technology*, Vol. 91, 2017, pp. 197–202.
[39] Zhao, Y. Co-precipitated Ni/Mn shell coated nano Cu-rich core structure: A phase-field study. *Journal of Materials Research Technology*, Vol. 21, 2022, pp. 546–560.
[40] Zhang, P., Z. Liu, X. Yue, P. Wang, and Y. Zhai. Water jet impact damage mechanism and dynamic penetration energy absorption of 2A12 aluminum alloy. *Vacuum*, Vol. 206, 2022, id. 111532.
[41] Zhang, P., Z. Liu, J. Liu, J. Yu, Q. Mai, and X. Yue. Effect of aging plus cryogenic treatment on the machinability of 7075 aluminum alloy. *Vacuum*, Vol. 208, 2023, id. 111692.
[42] Zhang, P., J. Liu, Y. Gao, Z. Liu, and Q. Mai. Effect of heat treatment process on the micro machinability of 7075 aluminum alloy. *Vacuum*, Vol. 207, 2023, id. 111574.
[43] Zhu, Z. Y., Y. L. Liu, G. Q. Gou, W. Gao, and J. Chen. Effect of heat input on interfacial characterization of the butter joint of hot-rolling CP-Ti/Q235 bimetallic sheets by Laser + CMT. *Scientific Reports*, Vol. 11, No. 1, 2021, id. 10020.
[44] Yang, J., S. Bai, J. Sun, H. Wu, S. Sun, S. Wang, et al. Microstructural understanding of the oxidation and inter-diffusion behavior of Cr-coated Alloy 800H in supercritical water. *Corrosion Science*, Vol. 211, 2023, id. 110910.
[45] Zhu, Q., J. Chen, G. Gou, H. Chen, and P. Li. Ameliorated longitudinal critically refracted—Attenuation velocity method for welding residual stress measurement. *Journal of Materials Processing Technology*, Vol. 246, 2017, pp. 267–275.
[46] Xu, H., T. He, N. Zhong, B. Zhao, and Z. Liu. Transient thermomechanical analysis of micro cylindrical asperity

sliding contact of SnSbCu alloy. *Tribology International*, Vol. 167, 2022, id. 107362.
[47] Liu, C., Y. Zhao, Y. Wang, T. Zhang, and H. Jia. Hybrid dynamic modeling and analysis of high-speed thin-rimmed gearsASME. *Journal of Mechanical Design*, Vol. 143, No. 12, 2021, id. 123401.
[48] Niu, X., S. Zhu, J. He, D. Liao, J. A. F. O. Correia, F. Berto, et al. Defect tolerant fatigue assessment of AM materials: Size effect and probabilistic prospects. *International Journal of Fatigue*, Vol. 160, 2022, id. 106884.
[49] He, J., S. Zhu, C. Luo, X. Niu, and Q. Wang. Size effect in fatigue modelling of defective materials: Application of the calibrated weakest-link theory. *International Journal of Fatigue*, Vol. 165, 2022, id. 107213.
[50] Li, X., S. Zhu, D. Liao, J. A. F. O. Correia, F. Berto, Q. Wang. Probabilistic fatigue modelling of metallic materials under notch and size effect using the weakest link theory. *International Journal of Fatigue*, Vol. 159, 2022, id. 106788.